Miniaturized and Flexible FSS based EM-Shields for Conformal Applications

Muhammad Bilal, Rashid Saleem, Qammer H. Abbasi *Senior Member IEEE,* Bakhtiar Kasi and M. Farhan Shafique, *Senior Member IEEE*

***Abstract*— This paper reports on very efficient and highly miniaturized wideband Polygon shaped Frequency Selective Surface (PFSS) shields for planar and conformal applications in X band. These shields have been analyzed for both lossy as well as for low loss substrates. The conformal configurations of PFSS are particularly investigated for inward, outward and double curved profiles useful for a variety of applications. The conformal designs have been tested for two different radii of curvatures. The models have been simulated using a hybrid simulation approach for electrically large geometries. Equivalent circuit model as well as analytical model is determined. The proposed PFSS designs offer stable angular response up to 60^0 for planar and all conformal geometries on both lossy and low loss prototypes. Shielding effectiveness of at least 55 dB and 48 dB has been measured for flat/non conformal and conformal configurations.**

***Index Terms*— Bandstop filters, Electromagnetic compatibility, Frequency Selective Surface (FSS), Interference, Shielding, Polarizations.**

I. Introduction

FREQUENCY selective surfaces (FSS) have been exhaustively investigated since the 1960s. An FSS is combination of a periodic structure designed to selectively absorb/reflect/transmit electromagnetic waves [1]. These surfaces can be referred to as spatial filters i.e. they can respond to a particular frequency in the whole electromagnetic spectrum [2]. Recent research trends lay emphasis on FSSs owing to their potential applications in; satellite communication services [6], antenna radomes [3], Radar Cross Section (RCS) reduction [4], efficient communication systems [5], performance enhancement of antennas, dichroic sub-reflectors, analog absorber and many others.

The performance of broadband communication systems that operate on low power spectral density and in particular portable communication devices are badly affected by electromagnetic interference (EMI). An efficiently designed FSS is a potential solution which not only mitigates interference but also maintains transparency to the rest of useful frequency spectrum. Planar FSS geometry can only be applied to flat surfaces thus various curved or pointed objects like cylinders or cones cannot be shielded. These kinds of applications demand for a conformal FSS shield which retains its performance when conformed around the desired object.

In recent literature, various planar and conformal FSS geometries are reported. In [8], A broadband flexible textile-integrated band stop FSS is presented. This large FSS achieves stable shielding response with a limited conformability. A flexible low profile Convoluted Ring Loop (CRL) FSS printed on Polyethylene Terephthalate (PET) is realized in [9] to achieve shielding at 10 GHz. This FSS achieves stable incident angular response for both Transverse Electric (TE) and Transverse Magnetic (TM) wave modes but up to 45^0 only. A dual band U-shaped FSS, reported in [10], effectively achieves EM shielding for X and Ku bands. In [11], a single-layer absorber containing two-dimensional array of cross dipoles are presented for RCS reduction. Another work shows band-stop FSS having a cross spiral shaped patch along with iterated H-shaped fractals arranged in the C-4 rotation to achieve polarization independent band-stop response [12]. In another study, a method of achieving wide range of beam widths by incorporating an outward curved conformal FSS in an antenna is presented [13]. Meandering technique makes this FSS significantly miniaturized and stable. In [14], flexible double-sided linear-to-circular polarizers are realized on polydimethylsiloxane. This configuration is based on two different unit cells, a loaded circular patch unit cell or an unloaded circular patch unit cell, both backed by a generic rectangular element. This double-sided polarizer achieves good phase difference, axial ratio (AR) and overall stable transmission response by employing inward and outward curved configurations. A couple of narrowband dielectric FSSs is reported in [15] to achieve reflection and transmission characteristics. In [16], a complementary symmetry is proposed to provide band-pass response. This complementary X-shaped FSS offers stable incident angular response along with miniaturized dimensions on a thin substrate. Electromagnetic shielding in X-band is achieved in [17] by realizing a convoluted square loop FSS on planar and curved flexible laminate. This analysis only investigates outward curved FSS surfaces. In [18], a miniaturized metamaterial based FSS is reported. This FSS is realized on a flexible ferrite laminate for generic microwave applications. A simple

Muhammad Bilal and Bakhtiar Kasi are with Department of Telecommunication Engineering, Balochistan University of IT, Engineering and Management Sciences, Quetta 87300, Pakistan

Rashid Saleem is with Department of Telecommunication Engineering, University of Engineering and Technology, Taxila 47080, Pakistan

Qammer H. Abbasi is with School of Engineering, University of Glasgow, Glasgow G12 8QQ, U.K

M. Farhan Shafique is with Center for Advance Studies in Telecommunications, COMSATS University Islamabad, Tarlai Kalan, Islamabad, 45550.Pakistan.

outward curved profile is investigated as an application. An active FSS is reported in [19] for beam switching applications. These slots based active FSSs are realized on a flexible substrate that circularly warps the dual band antenna for beam switching. In [20], a meandered loop based printed FSS is reported. The meandered profile of this FSS are optimized to design Radio Frequency (RF) planar shield for windows. The reported FSS offers optimum shielding while maintaining a stable incident angular response. Another single layer and dual band FSS design study is reported in [21]. The cross and ring shaped FSS are etched in a back-to-back planar configuration to achieve wide band shielding over limited angular stability. Another study reported in [22] reveals super formula-based creation of a dual band FSS where only planar configurations are desired. The super formula based square loop and inner ring achieves stable incident angular response while maintaining a miniaturized profile. In [23], a serpentine strip FSS based flexible shield is reported for flexible electronics. This flexible FSS shield incorporates all the design constraints while offering optimum shielding effectiveness when conformed only in inward configuration. Three ring slot pairs are reported in [24] for Ka-band radome applications. This reported FSS based radome offers flat passband response over a limited angular stability. In [25], a hybrid dual band FSS is reported. This configuration comprises of back-to-back arrangement of hexagonal patch in combination with hexagonal ring and Jerusalem cross. The reported design offers a narrowband reflective and transmissive response over Ku-band satellite and Ku-band active radars respectively. An ultra-wide stop-band single-layer FSS is reported in [26] to enhance the gain of an Ultra-Wideband (UWB) monopole antenna. The unit cell of the reported FSS consists of four asymmetric rectangular patches with circular slots embedded in it. This concept of four slotted patches is conceived to achieve ultra-wide stop-band characteristic with limited angular stability. In [27], a substrate integrated waveguide (SIW) technology based FSS is reported for airborne radome applications. This FSS consists of a tapered cross-slot on either side of the substrate surrounded by metallic vias. The structure selectively allows the impinging electromagnetic (EM) wave through it in the specified frequency band. The element shows very stable frequency response for oblique incidence and the narrow band roll-off performance characteristics at the edges of operating region in the stop band.

In the available literature, narrow band performance, lack of miniaturization, design complexity and incidence angular stability are the major limitations to overcome alongside. For conformal applications generally outward curved geometry is investigated.

The Polygon shaped Frequency Selective Surface (PFSS) proposed in this study addresses almost all the design constraints related to miniaturization, conformality and incident angle responses. The proposed PFSS effectively mitigates interference in X-band while maintaining stable incident angular performance up to 60^o in both polarization states. Planar and conformal shields including outward, inward, double curved configurations are designed and analyzed through the simplistic, quick and computationally less intensive full wave Finite Element Boundary Integral (FE-BI) system model [7]. Equivalent circuit model, analytical model and full wave analysis has been carried out to validate the shielding performance of the proposed PFSS.

Rest of the paper is organized as follows; geometrical configurations and evolution of the proposed flexible PFSS are presented in Section II. Design modeling and equivalent circuit model has been reported in Section III. Section IV presents parametric analysis and optimization of PFSS unit cell. Section V briefly explains the simulation setup for planar and conformal configuration. Measurement setup and measured results of shields are presented and compared in Section VI. Finally, Section VII concludes the paper

II. Geometrical Configuration

The unit cell design configuration of PFSS is presented in Fig. 1(a). This PFSS is simulated, fabricated and measured on two different substrates. For planar and non-conformal shield FR4 material (ε_r = 4.4, *tanδ* 0.02) is used to analyze the PFSS behavior in lossy substrate. For conformal shields Rogers 5880 (ε_r = 2.2, *tanδ* 0.0009) flexible laminate has been used. The periodic arrangement of the PFSS is illustrated in Fig. 1(b). The inter-element spacing of unit cells is optimized and fixed to $D_x = 0.3$ *mm* for both variants considering the fabrication limitations. Perspective view of the proposed FSS is presented in Fig. 1(c).

The proposed FSS geometry is mainly evolved through a 4-step design procedure as presented in Fig. 2. The unit cell comprises of twelve-sided polygon geometry. The total perimeter of the polygon is about λ_o at the resonant frequency as shown in Fig. 2a. An inflated X-shaped geometry having center width d_{r1} is etched in the center of polygon initially. This inflated X-shaped geometry mainly helps to achieve band-stop behavior at the desired frequency band as illustrated in Fig. 2b. It may be observed from the Fig. 2c that, the center width of inflated X-shaped geometry is further increased and optimized to achieve band-stop behavior at X-band centered at 10 GHz. The inner corners are rounded with radii d_{r3} to improve its angular repose and enhance bandwidth as shown in Fig 2d. The optimized geometry offers miniaturization as well as polarization independence owing to its symmetrical profile. The optimized dimensions including their optimization ranges are listed in Table I and Table II for both variations of design realized on Roggers 5880 and FR-4 laminate respectively.

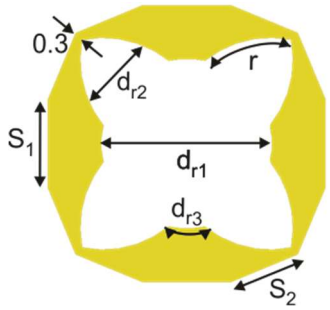

(a)

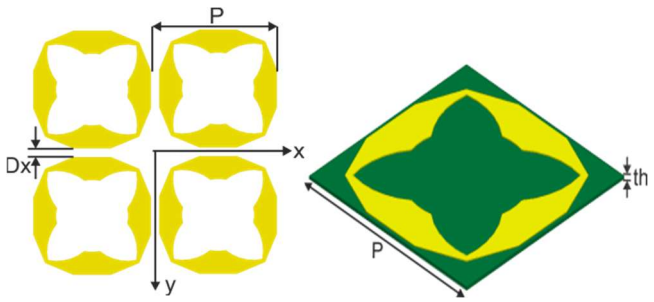

(b) (c)

Fig. 1. Layout of PFSS. (a) design configuration (b) array arrangement (c) perspective view

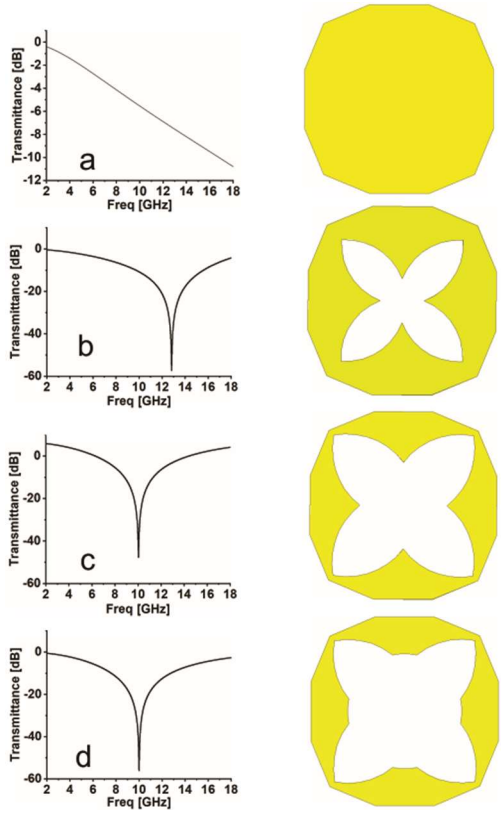

Fig. 2. Design procedure of the proposed PFSS

TABLE I
DIMENSIONS OF PFSS (ROGERS 5880)

Resonant Freq.: 10 GHz		
Variables	Optimization range (mm)	Optimized value (mm)
Length × *width*	7.5-8.5	8 × 8
d_{r1}	3-4.5	4
d_{r2}	1.5-2.6	2.2
d_{r3}	1.5-3	2.5
S_1	2-3	2.6
S_2	1.5-3	2.1
r	2.8-3.4	3.2
th	-	0.127
P	-	8.3

TABLE II
DIMENSIONS OF PFSS (FR-4)

Resonant Freq.: 10 GHz		
Variables	Optimization range (mm)	Optimized value (mm)
Length × *width*	6.8-7.8	7 × 7
d_{r1}	1.5-2.0	1.75
d_{r2}	0.5-1.5	1.2
d_{r3}	0.1-0.5	0.3
S_1	2-3	2
S_2	1.5-3	1.65
r	1.8-3.0	2.2
th	-	1.6
P	-	7.3

III. SIMULATIONS AND MODELING

Complete designing and optimization of the proposed PFSS is carried out in a commercially available 3D full wave electromagnetic simulator (Ansys HFSS®). The simulator solves Maxwell equations at the boundaries of tetrahedral mesh of the geometry. Floquet theory-based simulation setup was used for planar configuration with periodic boundary conditions whereas FE-BI simulation setup was used for conformal variants, more details on simulation setup is presented in Section V. Shielding Effectiveness (SE) of the proposed PFSS is expressed in (1), [17].

$$SE_{dB} = -20log\frac{E_t}{E_i} \quad (1)$$

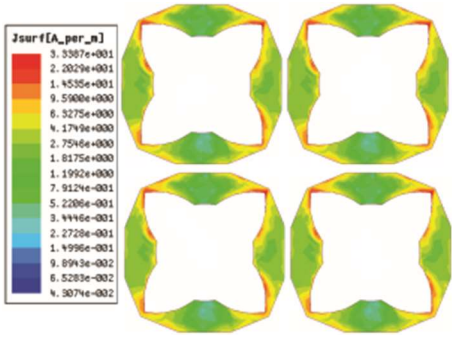

Fig. 3. Surface current distribution at 10 GHz.

The surface current density (J-surf) of this FSS array is examined at the resonant frequency of 10 GHz as shown in Fig. 3. The distribution reveals that current is more concentrated around the design corners. The significance of the inflated X geometry introduced in middle of the polygon is clear from this current distribution. The path of current can be increased or decreased by varying the shape without changing the overall size of polygon. The current intensity on metal introduces inductive effect, while the central X shape opening contributes to the capacitance.

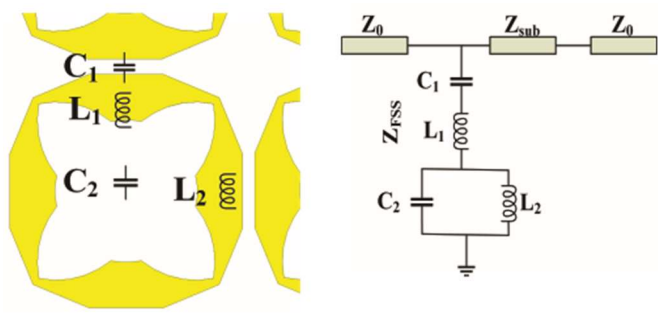

(a) (b)

Fig. 4. Equivalent circuit model of PFSS (a) lumped element formation (b) finalized ECM

An equivalent circuit model (ECM) of the proposed PFSS is developed to provide a physical interpretation of its performance determined by the full-wave simulations. The derivation of ECM mainly depends on the geometry of an FSS structure and the polarization of incident wave [22]. The surface current distribution on the proposed unit cell at 10 GHz under normal wave incidence (TEz-0°), also provide clues on the inductance and capacitance components in the equivalent circuit.

As a result, capacitances C_1 and C_2 are formed at the metallic gaps between PFSS unit cells and inflated X-shaped region. The inductances L_1 and L_2 are formed at the outer metallic edges of the PFSS as shown in Fig. 4a. The resultant ECM formation of the this FSS is presented in Fig. 4b. It may be observed from the Fig. 4b that, L_1 and C_1 are connected in series while parallel combination is visible between L_2 and C_2. The values of inductances and capacitances depend on the dimensions of FSS structure.

The free space on both sides of the unit cell is modeled as a transmission line with characteristic impedance of $Z_0 = 377\ \Omega$. The characteristic impedance of substrate is $Z_{sub} = \frac{Z_0}{\sqrt{\varepsilon_r}}$. The substrate thickness *th* and material characteristics affect the phase difference of incident wave [22].

The value of components of the equivalent circuit is determined by the use of final ECM transmission line model. The design analysis also reveals that due to the looping nature of geometry the increment in *L* and *C* lowers the resonant frequency. The proposed circuit model achieves band stop behavior at 10 GHz and its impedance is derived in (2).

The derived expression is categorized into two zeros and two poles. The relations for the lumped parameters are obtained by equating both the numerator and denominator of (2) equals to zero.

$$Z_{PFSS} = \frac{[\omega^2 C_1 L_2 - (1-\omega^2 C_1 L_1)(1-\omega^2 C_2 L_2)]}{j\omega C_1 (1-\omega^2 C_2 L_2)} \quad (2)$$

$$C_2 = \frac{1}{L_2 \omega_{p2}^2} \quad (3)$$

$$C_1 = \frac{(\omega_{p2}^2 - \omega_{z1}^2)(\omega_{p2}^2 - \omega_{z2}^2)}{-L_2 \omega_{p2}^2 \omega_{z1}^2 \omega_{z2}^2} \quad (4)$$

$$L_1 = \frac{(\omega_{p2}^2 - \omega_{z1}^2) - C_1 L_2 \omega_{p2}^2 \omega_{z1}^2}{C_1 \omega_{z1}^2 (\omega_{p2}^2 - \omega_{z1}^2)} \quad (5)$$

In the given equations (3), (4) and (5), ω_{p2}, ω_{z1} and ω_{z2} are the pole and two zeros respectively. Whereas, the first pole ω_{p1} is zero. The numerical value of L_2 has been inserted iteratively to evaluate rest of lumped parameters. The lumped parameters listed in Table. III, are calculated by using the above-mentioned relations.

TABLE III
LUMPED PARAMETERS

Equivalent circuit values			
C_1	C_2	L_1	L_2
0.03 pF	0.4 pF	0.9 nH	0.5 nH

The SE can be directly plotted using the equivalent circuit model shown in Fig 4 through an EDA tool. Alternatively, the transmission coefficient of the proposed PFSS can be approximated by transmission line theory (6), after evaluating the lumped parameters [28].

$$S_{21} = \frac{2Z_0}{AZ_0 + B + CZ_0^2 + DZ_0} \quad (6)$$

here coefficients: *A, B, C* and *D* refers to the *ABCD* matrix of the system having *N* number of FSS dielectric layers.

$$\begin{bmatrix} A & B \\ C & D \end{bmatrix} = [M_{PFSS}][M_{n+1}]..[M_N] \quad (7)$$

In 7, Mn is the scattering matrix of nth dielectric layer. Here in this particular design we have one dielectric layer on which the FSS design is resting thus the relation (7) is solved for single layer and it reduces to (8)

$$\begin{bmatrix} A & B \\ C & D \end{bmatrix} = [M_{PFSS}][M_1] \quad (8)$$

$$[M_1] = \begin{bmatrix} \cos(k_{z1}d) & jZ_o \sin(k_{z1}d) \\ j\frac{\sin(k_{z1}d)}{Z_o} & \cos(k_{z1}d) \end{bmatrix} \quad (9)$$

$$[M_{PFSS}] = \begin{bmatrix} 1 & 0 \\ 1/Z_{PFSS} & 1 \end{bmatrix} \quad (10)$$

Same procedure can be adapted for solving the TE and TM wave modes where Z_{PFSS} in (10) is replaced with Z^{TE} and Z^{TM} as given in (11) and (12) respectively.

$$Z^{TE} = \frac{(\omega \mu_r \mu_0)}{k_{z1}} \quad (11)$$

$$Z^{TM} = \frac{k_{z1}}{(\omega \varepsilon_r \varepsilon_0)} \quad (12)$$

Where k_{z1} and k_t are normal and tangential components of the wave number respectively and are given in (13) and (14). μ_r, μ_0 and ε_r, ε_0 are free space and relative magnetic permeabilities, and the free space and relative dielectric permitivities. Free space propagation constant is represented by k_0 and *d* represents the thickness of dielectric. The

incident angle of the wave striking the FSS surface is given by θ.

$$k_{z1} = \sqrt{\varepsilon_r k_0^2 - k_t^2} \quad (13)$$

$$k_t = k_0 \sin\theta \quad (14)$$

Comparison of SE simulated through unit cell Floquet's model along with SE simulated from circuit model and analytical model is presented in Fig 5. Excellent coherence can be observed in simulated and computed response.

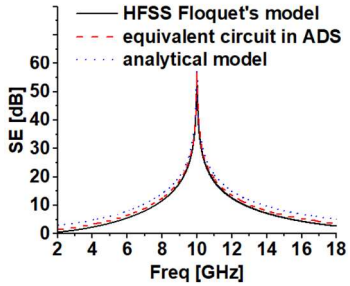

Fig. 5. SE comparison of HFSS vs. circuit model vs. analytical model

IV. Parametric Analysis and Design Optimization

A. Geometric analysis

The resonant frequency and SE are tuned by parametric optimization. Initially, the perimeter of the unit element is approximated at λ_o. Afterwards the optimum results have been achieved by tuning other parameters while maintaining the desired SE. The fine-tuning parameter of PFSS is the width of inflated X slot d_{r1}. It may be observed from the Fig. 6(a) that resonant frequency shifts to lower frequencies as central width d_{r1} increases by reducing the metallic surface area. The radius r and the gap d_{r2} of each corner are varied alongside to optimize the SE. The reduction in r and d_{r2} shifts resonant frequency towards higher frequencies as illustrated in Fig. 6(b). The thickness effect on SE of the employed laminate is also investigated in Fig. 6(c). It may be noticed that, the reduction in thickness, shifts the resonant frequency to higher frequencies. Overall, SE of not less than 55 dB is observed for PFSS while maintaining miniaturized dimensions and wideband response.

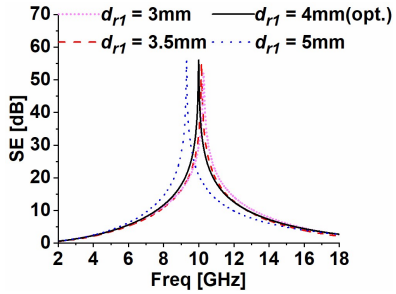

(a)

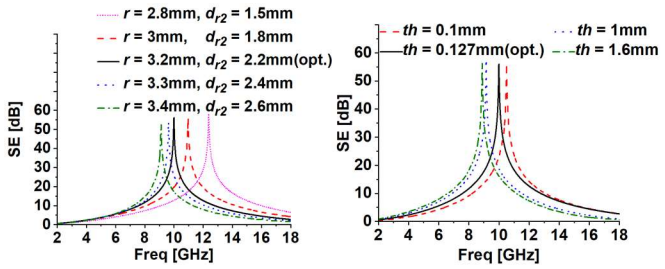

(b) (c)

Fig. 6. PFSS parametric optimization. (a) center width d_{r1} variations (b) corner width d_{r2} along with radii r variation (c) thickness th variation

B. Substrate Analysis

The relative permittivity of the employed laminate is varied to investigate its effect on the performance of PFSS. It may be observed from the Fig. 7 that; resonant frequency tends to shift from higher to lower frequencies as ε_r increases. This is true since the electrical length of resonant element is inversely related to the square root of dielectric constant.

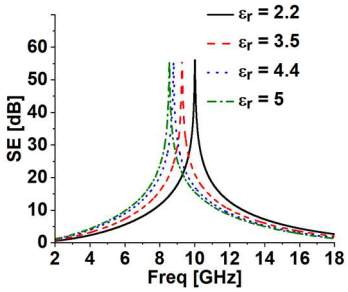

Fig. 7: Relative Permittivity effects on resonant frequency.

The dielectric loss tangent *tan δ* of employed laminate is also varied to study its effect on overall shielding response. As shown in Fig. 8, SE exponentially decreases as the loss tangent increase from 0.009 to 0.5. It happens because the resonant elements fail to efficiently resonate at the desired frequency due to higher loss.

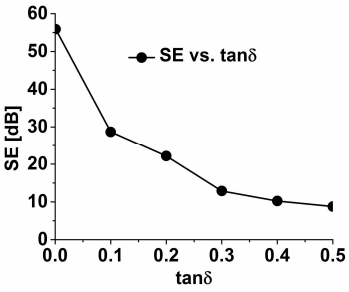

Fig. 8. Dielectric loss tangent (tanδ) performance

V. Simulation Setup For Planar and Conformal Designs

For planar designs the periodic boundary conditions can be employed therefore the incident angular performance of the proposed unit cell of PFSS is investigated by employing Floquet's method. A unit cell is assigned periodic boundary conditions and it is excited though a Floquet port to simulate the infinite periodicity. The SE is simulated up to an angle of

60^0 for both TE and TM modes. It is also worth mentioning that the element separation is much smaller than operating wavelength so only fundamental Floquet mode shall exist at the operating frequency. It can also be ensured from the relation (15). Where $\lambda_g^{\varepsilon_r}$ shows the wavelength of the first higher order harmonic of floquet mode and θ is the incident angle.

$$\lambda_g^{\varepsilon_r} = D_x\left(\sqrt{\varepsilon_{r_{eff}}} + \sin\theta\right) \quad (15)$$

The conceptual view of conformal configurations is presented in Fig. 9. The simulation setup of conformal shield is not straight forward since the field distributions are not symmetric on the left/right and top/bottom boundaries of a unit cell therefore Floquet method cannot be applied. A conventional free space simulation setup can be used but owing to electrically large geometry the computations complexity will increase multifold. Therefore, the conformal configurations have been analyzed by employing hybrid full wave FE-BI system model. Full wave simulation setup for analyzing all conformal PFSS shields is presented in Fig. 10. Each shield contains 25 × 25 unit elements and is placed between transmitting and receiving horn antennas. These horns are designed and optimized to operate in X-band (8 – 12 GHz). FE-BI boundary conditions are assigned to PFSS array/shield and both horn antennas. Owing to the closer boundaries, the overall free space region is reduced which results in faster simulation [7]. These full wave simulations took about 14 hours with 18 GB of RAM on Xeon E5-1650 hexa core CPU clocked at 3.5 GHz.

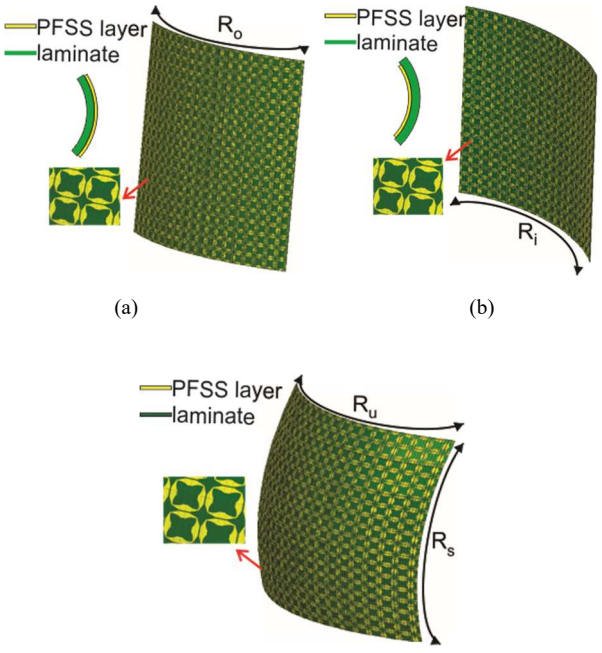

Fig. 9. 3D conceptual view of conformal configuration. (a) outward curved (b) inward curved (c) double curved

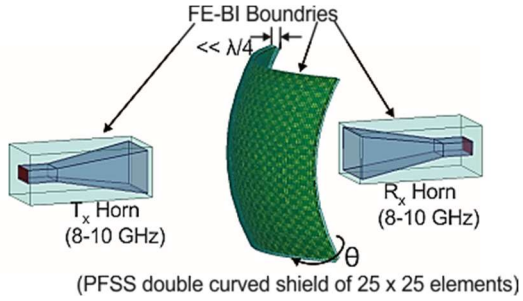

Fig. 10. FE-BI simulation setup for PFSS double curved shield

VI. MEASUREMENT SETUP AND RESULTS

Full wave simulated results of planar and conformal PFSS shields are validated by employing free space measurement setup illustrated in Fig. 11. A $7.5\lambda_0 \times 10\lambda_0$ planar and conformal PFSS shields are fabricated on FR-4 and flexible Rogers 5880 with thickness of 1.6 mm and 0.127 mm respectively as illustrated in Fig. 12. An aluminum wall with an aperture in the middle has been used for measurements. These shields are fixed in the aperture one-by-one so that all radiations only pass from the shield. A pair of Lucas Nuelle WR90 15 dBi horn antennas operating in X-band is placed in the far field on both sides which are connected to Agilent PNA N5242A network analyzer. The employed measurement setup is initially calibrated to normalize the reference transmission level through the empty aperture.

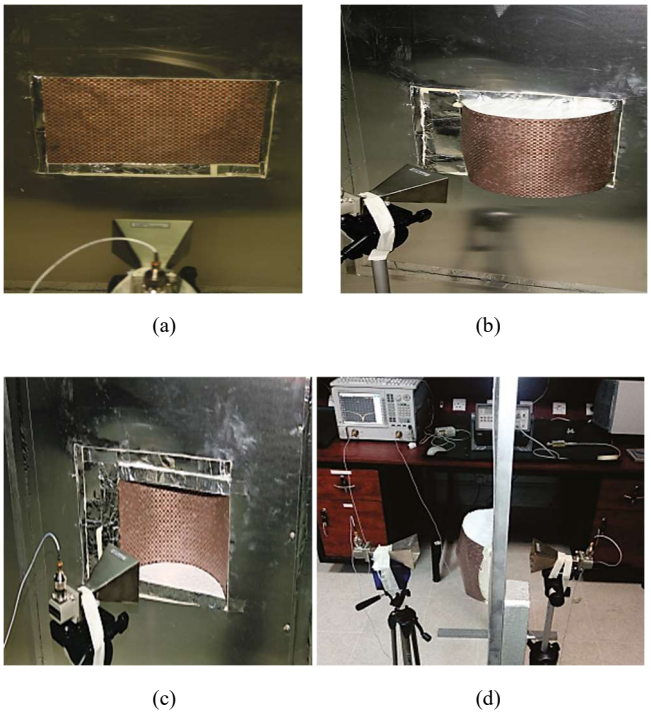

Fig. 11. Shielding measurements of PFSS shield on flexible laminate (a) non-conformal / flat PFSS shield under measurement. (b) outward curved PFSS shield (c) inward curved PFSS shield (d) double curved PFSS shield under measurement.

Once the calibration was completed planar and conformal PFSS shields were installed in the aperture between these antennas to measure their shielding effectiveness. Multiple

measurements were performed to check variability/uncertainty (δ) in the measured results [29]. Overall, $\delta = \pm 0.06, \delta = \pm 0.05$, $\delta = \pm 0.08$ and $\delta = \pm 0.1$ is observed for flat, outward, inward and double curved shield measurements respectively. This slight variation in measured results may be observed due to sensitivity of FSS for small changes, curved profile, fabrication imperfections and possible errors in measurement setup.

(a) (b)

Fig. 12. Fabricated PFSS shield on flexible laminate (a) non-conformal / flat PFSS shield (b) double curved PFSS shield.

A. *Planar PFSS shield realized on FR-4*

Simulated and measured SEs of planar PFSS shield are compared for both TE and TM wave modes as presented in Figs. 13(a) and 13(b). The proposed planar shields achieve SE of more than 40 dB while maintaining a wideband response. Additionally, measured shielding response for oblique incidences is presented in Figs. 13(c) and 13(d). The results reveal that the bandwidth increases slightly and resonant frequency slightly decreases and shifts about 2% as the angle of incidence increases. Overall, simulated results are in line with measurements.

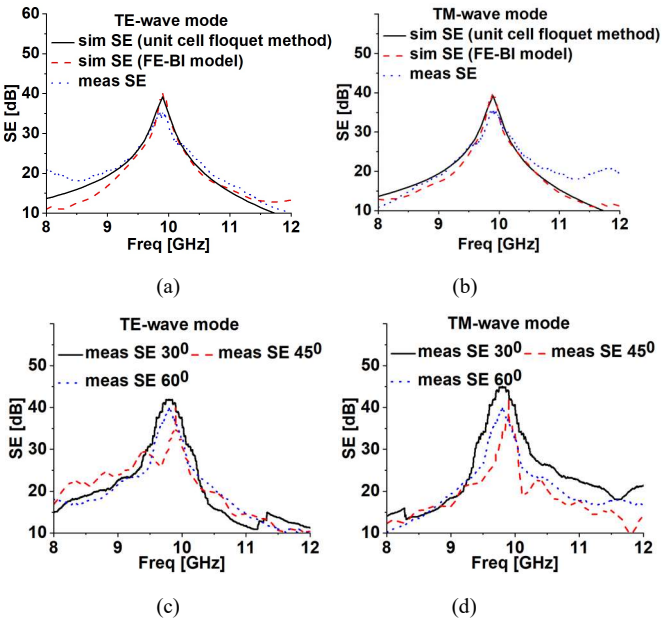

(a) (b)

(c) (d)

Fig. 13. Simulated vs. measured normal and oblique SE for planar PFSS shield realized on FR4. (a) (c) TE-wave mode, (b) (d) TM-wave mode

B. *PFSS shield realized on Rogers 5880*

The SE of the low loss laminate based PFSS shield is compared for simulated and measured responses as shown in Figs. 14(a) and 14(b). The FSS shield achieves SE of not less than 55 dB. However, 2% variation is observed in measurements as the angle of incidence increases up to 60^0 as illustrated in Figs. 14(c) and 14(d)

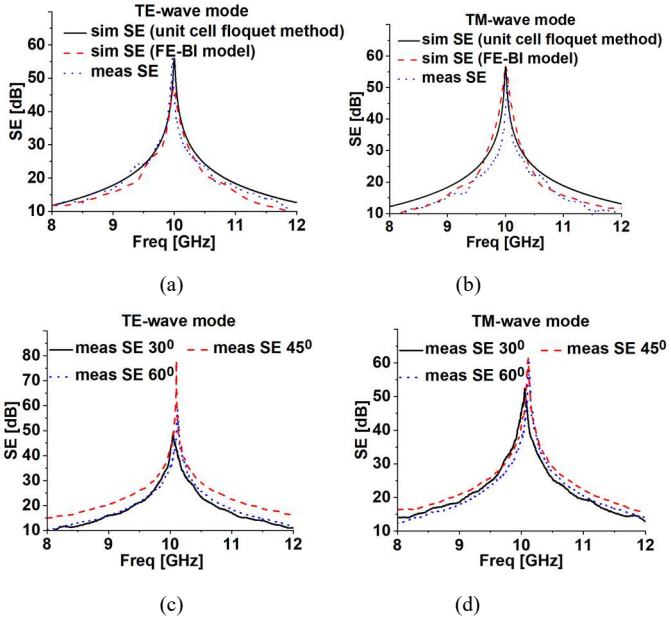

(a) (b)

(c) (d)

Fig. 14. Simulated vs. measured normal and oblique SE for flat PFSS shield realized on 5880. (a) (c) TE-wave mode, (b) (d) TM-wave mode

C. *Conformal Configurations*

The Proposed PFSS shield is conformed in three configurations for conformal applications. The testing setup for conformal configurations for normal as well as oblique angles is presented in Figs. 11(b), 11(c) and 11(d). Calibration is again performed prior to testing of all conformal shields.

1) *Outward curved PFSS shield*

The shielding response of outward curved shield is evaluated and compared with full wave simulations by varying the radius of curvature R_o (Fig 9a). The shielding behavior of the proposed outward curved PFSS shield is presented in Fig. 15. It may be observed that, SE is slightly reduced to 50 dB and shifts only 1% and 2% from the resonant frequency of 10 GHz, as the radius R_o reduces from 12cm to 6cm respectively. The incident angular performance of this conformal configuration is illustrated in Figs. 15(c) and 15(d). The oblique performance is evaluated by varying θ up to 60^0 at both variations of R_o. The SE shifts only 2% as the angle of incidence increases for both TE and TM-wave mode at both variations of R_o. Overall, this configuration exhibits stable incident angular behavior in all variations.

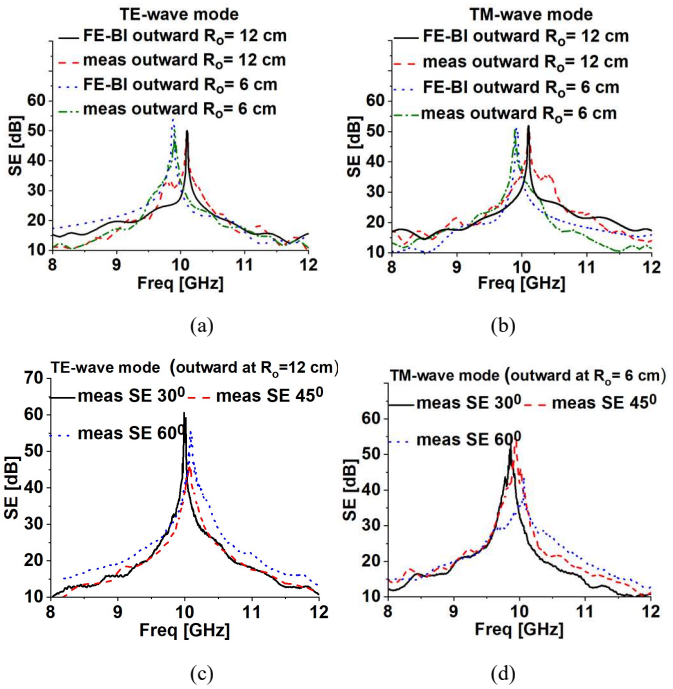

Fig. 15. Simulated vs. measured normal and oblique SE of outward curved PFSS shield. (a) (c) TE-wave mode, (b) (d) TM-wave mode

2) Inward curved PFSS shield

A good agreement between simulated and measured shielding performance is observed for the proposed inward curved PFSS shield as shown in Figs. 16(a) and 16(b). This curved configuration also offers SE of not less than 50 dB while maintaining a wideband response. SE shifts only 1% from the resonant frequency for both curved variations of the arc having radius R_i.

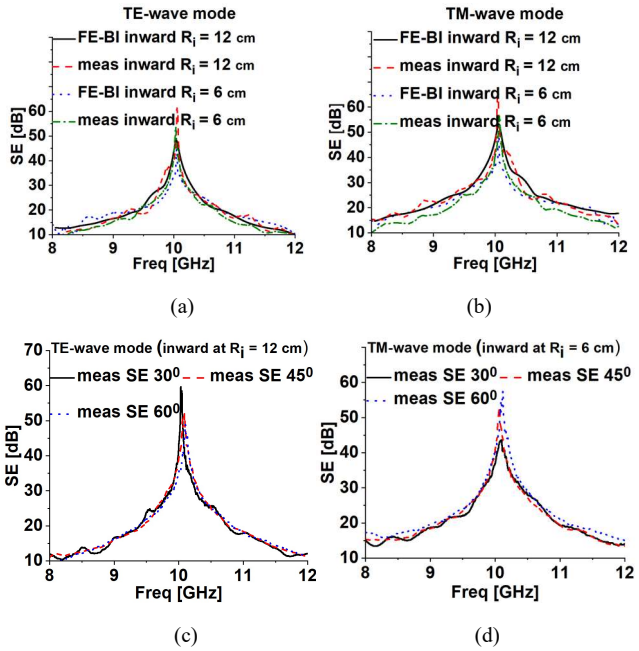

Fig. 16. Simulated vs. measured normal and oblique SE of inward curved PFSS shield. (a) (c) TE-wave mode, (b) (d) TM-wave mode

A stable incident angular response is observed in general for this configuration with a minor shift of 1% at oblique incidences as illustrated in Figs. 16(c) and 16(d).

3) Double curved PFSS shield

Measured shielding performance of double curved shield is presented in Figs. 17(a) and 17(b). It may be observed that, SE shifts only 3% for both variations of R_u and R_s. Moreover, a slight decrease in SE is also observed due to highly conformal surface. This configuration achieves SE of not less than 48 dB besides having highly conformal nature. The oblique incidence performance of this shield is illustrated in Figs. 17(c) and 17(d). The, SE varies only 3% from the resonant frequency when the angle of incidence increases up to 60^0. Overall, this conformal configuration also exhibits stable incident angular response within acceptable limits.

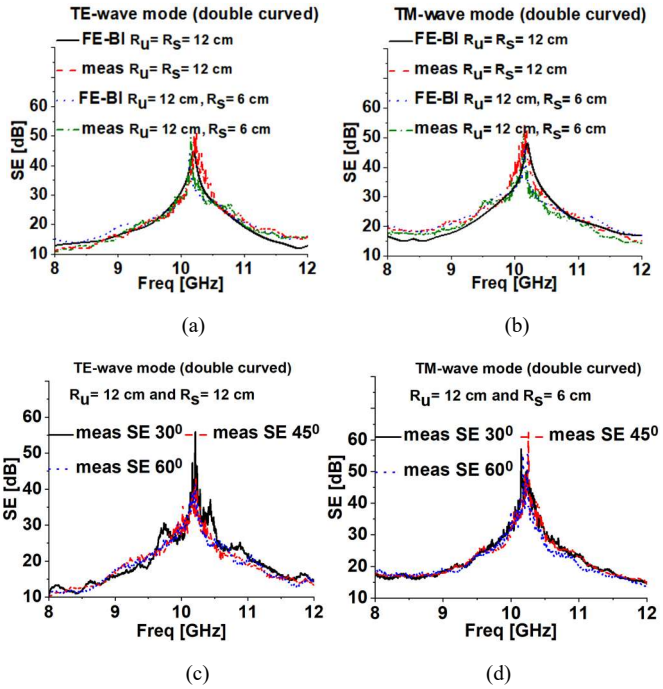

Fig. 17. Simulated vs. measured normal and oblique SE of double curved PFSS shield. (a) (c) TE-wave mode, (b) (d) TM-wave mode

D. Non-conformal vs. conformal

The measured shielding performance of the proposed PFSS shield in flat and conformal configurations is compared in Fig. 18. It may be noticed that, SE is shifted less than 3% when PFSS is bent. These variations are attributed to curved profile and non-regular shape. However, this shift can be conveniently compensated at the design phase by considering the intended application. In general, this conformal shield exhibits stable shielding performance of not less than 55 dB and 48 dB for non-conformal/flat and conformal configurations respectively.

TABLE IV
COMPARISON WITH PREVIOUS WORK

Ref.	Size		Freq. (GHz)	ε_r	Shielding (dB)		Conformal config.	Ang. stability	Ang. variation	Full wave Analysis
	Free space wavelengths λ_0	Guided wavelengths Λ_g			Flat	Conformal				
[8]	0.51	0.39	3.4 and 5.1	1.7	<50	<40	Outward curved	Up to 45^0	4%	yes
[9]	0.25	0.15	10	2.7	<36	35	Outward curved	Up to 45^0	<4%	No
[17] Author's previous work	0.21	0.15	10	2.2	56	<48	Outward curved	Up to 60^0	3%	No
[18]	0.21	0.06	2.56	10	25	25	Outward curved	-	-	No
[20]	0.10	0.04	2	3.4	38	-	-	Up to 60^0	2%	No
[21]	0.26	0.12	6.5 and 14	4.4	35	-	-	Up to 45^0	2%	No
[22]	0.11	0.05	3.46 and 5.14	4.3	<38	-	-	Up to 60^0	>2%	No
[23]	0.27	0.14	9.5	3.5	<25	<40	Inward curved	Up to 60^0	<3%	Yes
This work	**0.26 (on 5880)**	**0.17**	**10**	**2.2**	**55**	**48**	**Outward, inward and double curved**	**Up 60^0**	**<3%**	**Yes**

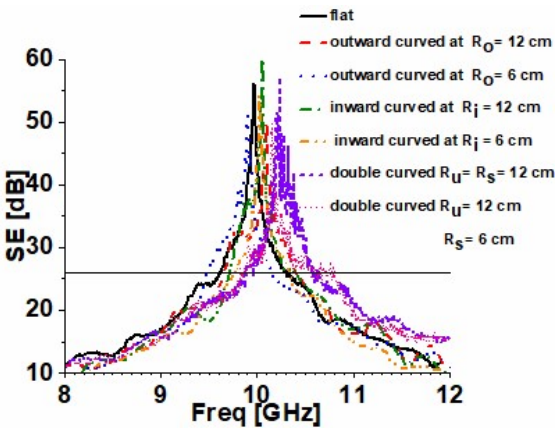

Fig. 18. Measured flat vs. conformal configurations

E. Comparison with existing literature

Table IV gives a comparison of metrics for the proposed FSS with those available in the literature. From the comparison table, it is evident that, the most closely related works shows the good shielding performance and angular stability up to 45^0 either for flat, outward or inward curved configuration while maintaining low-profile design aspects. However, the higher degree of incidence angle tolerance is essential for the FSS and it is difficult to achieve over a highly conformal surface while achieving a good shielding performance and miniaturization alongside. The proposed FSS exhibits a higher order of angular stability up to 60^0 for highly conformal configurations including outward, inward and double curved. Moreover, relatively miniaturized single-layer unit cell structure, with good shielding characteristics are also the main advantages of the proposed FSS in comparison to the previously published works.

VII. CONCLUSION

This paper presented efficient and highly flexible PFSS based EM shields. The effectiveness of these shields is demonstrated for both planar and conformal configurations in order to serve a wide variety of applications. The design is simple in making and offers good shielding with at least 55 dB and 48 dB suppression at the resonant frequency for flat and all conformal configurations respectively. More importantly, a stable incident angular performance for both polarizations is also demonstrated for all variants under a wide range of incident angles up to 60^0. The prototypes of all the proposed PFSS shields are fabricated and tested to verify their performance. SE of each configuration only varies a little as compared to simulations which can be priorly compensated at the design stage considering the intended application. The measurements are in line with the simulated full-wave analysis, hence making it a potential candidate for X-band planar and conformal applications including but not limited to SATCOMs, frequency selective radomes, high impedance surfaces (HISs), reduction of radar cross section of aerial vehicles and many others.

REFERENCES

[1] B. A. Munk, Frequency Selective Surfaces: Theory and Design. Hoboken,NJ, USA: Wiley, 2000

[2] T. K. Wu, Frequency selective surface and grid array. Wiley-Interscience, 1996, vol. 40.

[3] S. Narayan, G. Gulati, B. Sangeetha and R. U. Nair, "Novel Metamaterial-Element-Based FSS for Airborne Radome Applications," IEEE Transactions on Antennas and Propagation, vol. 66, no. 9, pp. 4695-4707, 2018.

[4] S. R. Thummaluru, R. Kumar and R. K. Chaudhary, "Isolation Enhancement and Radar Cross Section Reduction of MIMO Antenna With Frequency Selective Surface," *IEEE Transactions on Antennas and Propagation*, vol. 66, no. 3, pp. 1595-1600, 2018.

[5] M. Bilal, R. Saleem, H. H. Abbasi, M. F. Shafique and A. K. Brown, "An FSS-Based Nonplanar Quad-Element UWB-MIMO Antenna System," *IEEE Antennas and Wireless Propagation Letters*, vol. 16, pp. 987-990, 2017

[6] M. Bilal, R. Saleem, T. Shabbir, M. Farhan Shafique. "A novel miniaturized FSS based electromagnetic shield for SATCOM applications," *Microw Opt Technol Lett*., vol. 59, pp. 2107–2112, 2017.

[7] J. F. Mologni, M. Kopp, C. L. R. Siqueira, A. Colin, A. Nogueira, and M. A. R. Alves, "Automotive emc analysis using the hybrid finite element boundary integral approach," *IEEE International Symposium on Electromagnetic Compatibility*, pp. 688-693, 2013.

[8] L. Alonso-González, S. Ver-Hoeye, M. Fernández-García and F. Las-Heras Andrés, "Broadband Flexible Fully Textile-Integrated Bandstop Frequency Selective Surface," *IEEE Transactions on Antennas and Propagation*, vol. 66, no. 10, pp. 5291-5299, Oct. 2018.

[9] W. Y. Yong, S. K. Abdul Rahim, M. Himdi. F. C. Seman, D. L. Suong, M. R. Ramli and H. A. Elmobarak, "Flexible Convoluted Ring Shaped FSS for X-Band Screening Application," *IEEE Access,* vol. 6, no., pp. 11657-11665, 2018.

[10] M. Bakir, K. Delihacioglu, M. Karaaslan, F. Dincer, and C. Sabah, "U-shaped frequency selective surfaces for single- and dual-band applications together with absorber and sensor configurations," *IET Microwaves, Antennas Propagation*, vol. 10, no. 3, pp. 293-300, 2016.

[11] D. Kundu, A. Mohan, and A. Chakrabarty, "Single-layer wideband microwave absorber using array of crossed dipoles," *IEEE Antennas and Wireless Propagation Letters*, vol. 15, pp. 1589-1592, 2016.

[12] Z. Zhao, H. Shi, J. Guo, W. Li, and A. Zhang, "Stopband frequency selective sur- face with ultra-large angle of incidence," *IEEE Antennas and Wireless Propagation Letters*, vol. 16, pp. 553-556, 2017.

[13] A. Chatterjee and S. K. Parui, "Beamwidth Control of Omnidirectional Antenna Using Conformal Frequency Selective Surface of Different Curvatures," *IEEE Transactions on Antennas and Propagation*, vol. 66, no. 6, pp. 3225-3230, 2018.

[14] H. Mirza, T. M. Hossain, P. J. Soh, M. F. Jamlos, M. N. Ramli, A. A. Al-Hadi, E. S. Hassan and S. Yan, "Deployable Linear-to-Circular Polarizer Using PDMS Based on Unloaded and Loaded Circular FSS Arrays for Pico-Satellites," *IEEE Access*, vol. 7, no., pp. 2034-2041, 2019.

[15] A. Coves, S. Marini, B. Gimeno, D. SA¡nchez, A. RodrAguez, and V. E. Boria, "Design of narrow-band dielectric frequency-selective surfaces for microwave *applications," IET Microwaves, Antennas Propagation*, vol. 10, no. 3, pp. 251-255, 2016.

[16] H. Li, C. Yang, Q. Cao, and Y. Wang, "An ultrathin bandpass frequency selective surface with miniaturized element," *IEEE Antennas and Wireless Propagation Letters*, vol. 16, pp. 341-344, 2017.

[17] M. Nauman, R. Saleem, A. K. Rashid, and M. F. Shafique, "A miniaturized flexible frequency selective surface for x-band applications," *IEEE Transactions on Electromagnetic Compatibility*, vol. 58, no. 2, pp. 419-428, 2016.

[18] B. Gao, M. M. F. Yuen, and T. T. Ye, "Flexible frequency selective metamaterials for microwave applications," Scientific Reports, vol. 7, 2017.

[19] C. Gu, B. S. Izquierdo, S. Gao, J. C. Batchelor, E. A. Parker, F. Qin, G. Wei, J. Li, and J. Xu, "Dual-band electronically beam-switched antenna using slot active frequency selective surface," *IEEE Transactions on Antennas and Propagation*, vol. 65, no. 3, pp. 1393-1398, 2017.

[20] A. A. Dewani, S. G. O'Keefe, D. V. Thiel and A. Galehdar, "Window RF Shielding Film Using Printed FSS," in IEEE Transactions on Antennas and Propagation, vol. 66, no. 2, pp. 790-796, 2018.

[21] I. S. Syed, Y. Ranga, L. Matekovits, K. P. Esselle and S. Hay, "A Single-Layer Frequency-Selective Surface for Ultrawideband Electromagnetic Shielding," in IEEE Transactions on Electromagnetic Compatibility, vol. 56, no. 6, pp. 1404-1411, 2014.

[22] S. Khajevandi, H. Oraizi and M. Poordaraee, "Design of Planar Dual-Bandstop FSS Using Square-Loop-Enclosing Superformula Curves," in IEEE Antennas and Wireless Propagation Letters, vol. 17, no. 5, pp. 731-734, 2018

[23] S. Chen et al., "Flexible Serpentine like Frequency Selective Surface for Conformal Applications With Stable Frequency Response," in IEEE Antennas and Wireless Propagation Letters, vol. 18, no. 7, pp. 1477-1481, 2019.

[24] W. Wu, X. Liu, K. Cui, Y. Ma and Y. Yuan, "An Ultrathin and Polarization-Insensitive Frequency Selective Surface at Ka-Band," in IEEE Antennas and Wireless Propagation Letters, vol. 17, no. 1, pp. 74-77, 2018.

[25] Y. Ma, W. Wu, Y. Yuan, W. Yuan and N. Yuan, "A High-Selective Frequency Selective Surface With Hybrid Unit Cells," in IEEE Access, vol. 6, pp. 75259-75267, 2018.

[26] P. Das and K. Mandal, "Modelling of ultra-wide stop-band frequency-selective surface to enhance the gain of a UWB antenna," in IET Microwaves, Antennas & Propagation, vol. 13, no. 3, pp. 269-277, 2019.

[27] V. Krushna Kanth and S. Raghavan, "EM Design and Analysis of Frequency Selective Surface Based on Substrate-Integrated Waveguide Technology for Airborne Radome Application," in IEEE Transactions on Microwave Theory and Techniques, vol. 67, no. 5, pp. 1727-1739, 2019.

[28] F. Costa, A. Monorchio, and G. Manara, "An overview of equivalent circuit mod- eling techniques of frequency selective surfaces and metasurfaces," *ACES Journal*, vol. 29, no. 12, pp. 960-976, 2014.

[29] D. C. Baird, Experimentation: An Introduction to Measurement Theory and Experiment Design, 3rd. ed. Prentice Hall: Englewood Cliffs, 1995.

Muhammad Bilal received his B.S degree in Telecommunication Engineering in 2011 from Baluchistan University of Information Technology, Engineering and Management Sciences (BUITEMS), Quetta, Pakistan. He availed fully funded scholarship for Masters in Telecommunication Engineering in 2014 from University of Engineering and Technology (UET) Taxila, Pakistan. In 2018, he received the Ph.D. degree from the UET Taxila with specialization in Antennas and Electromagnetics. Since Feb 2018, he is perusing his career as an Assistant Professor with the Department of Telecommunication Engineering (BUITEMS), where he is heading Higher Education Commission (HEC) funded research project while supervising graduate and post-graduate students. His current research interests include UWB-MIMO systems, High gain portable devices, Frequency Selective Surfaces and Reflectarrays. He has published in many reputable scientific journals and conferences

Rashid Saleem received BS electronic engineering from Ghulam Ishaq Khan Institute of Engineering Sciences and Technology, Pakistan, in 1999. He pursued a career in the telecommunication industry for several years while continuing education. He received M.S. from UET Taxila through Center for Advanced Studies in Engineering, Pakistan, in 2006 and PhD from The University of Manchester, United Kingdom in 2011. He worked on antennas, channel modeling and interference aspects of Ultra Wideband systems during his PhD and was also member of a team designing and testing arrays for the Square Kilometer Array project. Currently, he is working as Assistant Professor at University of Engineering and Technology (UET), Taxila, Pakistan where he is supervising several postgraduate students and heading the MAP (Microwave Antennas and Propagation) research group. His research interests include antennas,

angle-of-arrival based channel modeling, microwave periodic structures and metamaterial.

Qammer H. Abbasi (SM'16) received the B.Sc. and M.Sc. degrees (Hons.) in electronics and telecommunication engineering from the University of Engineering and Technology (UET), Lahore, Pakistan, and the Ph.D. degree in electronic and electrical engineering from the Queen Mary University of London(QMUL), U.K., in 2012. In 2012, he was a Post-Doctoral Research Assistant with the Antenna and Electromagnetics Group, QMUL. From 2012 to 2013, he was inter-national young Scientist under the National Science Foundation China, and an Assistant Professor with UET, KSK, Lahore. From 2013 to 2017, he was with the Centre for Remote Healthcare Technology and Wireless Research Group, Department of Electrical and Computer Engineering, Texas A&M University (TAMUQ) initially as an Assistant Research Scientist and later was promoted to an Associate Research Scientist and a Visiting Lecturer, where he was leading multiple Qatar national research foundation grants (worth 3 million). He is currently a Lecturer (Assistant Professor) with the School of Engineering, University of Glasgow, U.K., in addition, he is also a Visiting Research Fellow with QMUL and a Visiting Associate Research Scientist with TAMUQ. He has been mentoring several undergraduate, graduate students, and post-docs. He has contributed to a patent, over 150 leading international technical journal, peer reviewed conference papers, and ve books. He has also received several recognitions for his research including the University Research Excellence Award from TAMUQ in two consecutive years, the Reward for Exellence from the University of Glasgow, exceptional talent endorsement (awarded to early career world-leading innovators and scientists) by the Royal Academy of Engineering, and most downloaded paper in the IEEE TERAHERTZ TRANSACTION. Media coverage by Analog IC tips, Microwaves & RF Newsletters, Vertical News. His research interests include compact antenna design, RF design and radio propagation, nano communication, biomedical applications of terahertz communication, antenna interaction with human body, implants, body centric wireless communication issues, wireless body sensor networks, non-invasive health care solutions, cognitive and cooperative network, and multiple-input-multipleoutput systems. He has been a member of the technical program committees of several IEEE agship conferences. He is an Associate Editor for the IEEE ACCESS journal, the IEEE JOURNAL OF ELECTROMAGNETICS, RF AND MICROWAVES IN MEDICINE AND BIOLOGY and acted as a guest editor for numerous special issues in top notch journals. He has been a technical reviewer for several IEEE and top-notch journals. He contributed in organizing several IEEE conferences, workshop, and special sessions in addition to European school of antenna.

Bakhtiar Kasi is a IEEE professional member (IEEE # 90608299). Dr. Kasi received Ph.D. degree in Computer Science from University of Nebraska-Lincoln, USA, in Dec 2015. He received his M.S. degree in Computer Science from SZABIST, Karachi, and B.E. in Software Engineering from Bahria University, Karachi. He is currently serving as the Dean Faculty of Information and Communication Technology at BUITEMS, Quetta. His research interests include machine learning, information retrieval, constraint processing, static analysis, and 'big data' analysis; more specifically, he has worked in multi-label classifications, SMT solving, and natural language processing. Dr. Kasi is Co-PI of the National Center for AI and Robotics. He has presented his research at top-tier international conferences on software engineering, and has also served on program committees, and co-reviewed papers in international conferences. He is also a recipient of the Fulbright Ph.D. scholarship award.

Muhammad Farhan Shafique (S'08–M'11–SM'15) received the B.Eng. degree from Hamdard University, Karachi, Pakistan, in 2003, M.S. degree from the University of Paris East Marne-La-Vallee, Paris, France, in 2005 and PhD in electronic and communications engineering from The University of Leeds, Leeds, U.K in 2010. His research interests involve multilayered-microwave device fabrication on LTCC and thick-film technology, RF antenna and antenna arrays, ultra wideband diversity antennas and MEMS packaging. He is also involved in dielectric characterization of materials using microwave techniques and fabrication of ceramic microfluidic devices. From 2007 to 2010 he was involved in establishing the LTCC fabrication facility at Institute of Microwave and Photonics, The University of Leeds, UK. He has extensive experience of laser micromachining and multilayer LTCC device modeling and fabrication. He is working as an Associate Professor at COMSATS University Islamabad (CUI), Pakistan. He is founder head of MCAD research group, Associate Director of Center for Advanced Studies in Telecommunications.